Biomaterials 245 (2020) 119973

Contents lists available at ScienceDirect

Biomaterials

journal homepage: www.elsevier.com/locate/biomaterials

Multi-peptide presentation and hydrogel mechanics jointly enhance therapeutic duo-potential of entrapped stromal cells

Ben P. Hung[a,1], Tomas Gonzalez-Fernandez[a,1], Jenny B. Lin[a,b], Takeyah Campbell[a], Yu Bin Lee[c], Alyssa Panitch[a], Eben Alsberg[c], J. Kent Leach[a,d,**]

[a] Department of Biomedical Engineering, University of California, Davis, Davis, CA, USA
[b] Weldon School of Biomedical Engineering, Purdue University, West Lafayette, IN, USA
[c] Department of Biomedical Engineering, University of Illinois, Chicago, IL, USA
[d] Department of Orthopaedic Surgery, UC Davis Health, Sacramento, CA 95817, USA

ARTICLE INFO

Keywords:
Stress relaxation
Alginate
Angiogenesis
Osteogenesis
Mesenchymal stromal cells

ABSTRACT

The native extracellular matrix (ECM) contains a host of matricellular proteins and bioactive factors that regulate cell behavior, and many ECM components have been leveraged to guide cell fate. However, the large size and chemical characteristics of these constituents complicate their incorporation into biomaterials without interfering with material properties, motivating the need for alternative approaches to regulate cellular responses. Mesenchymal stromal cells (MSCs) can promote osseous regeneration *in vivo* directly or indirectly through multiple means including (1) secretion of proangiogenic and mitogenic factors to initiate formation of a vascular template and recruit host cells into the tissue site or (2) direct differentiation into osteoblasts. As MSC behavior is influenced by the properties of engineered hydrogels, we hypothesized that the biochemical and biophysical properties of alginate could be manipulated to promote the dual contributions of encapsulated MSCs toward bone formation. We functionalized alginate with QK peptide to enhance proangiogenic factor secretion and RGD to promote adhesion, while biomechanical-mediated osteogenic cues were controlled by modulating viscoelastic properties of the alginate substrate. A 1:1 ratio of QK:RGD resulted in the highest levels of both proangiogenic factor secretion and mineralization *in vitro*. Viscoelastic alginate outperformed purely elastic gels in both categories, and this effect was enhanced by stiffness up to 20 kPa. Furthermore, viscoelastic constructs promoted vessel infiltration and bone regeneration in a rat calvarial defect over 12 weeks. These data suggest that modulating viscoelastic properties of biomaterials, in conjunction with dual peptide functionalization, can simultaneously enhance multiple aspects of MSC regenerative potential and improve neovascularization of engineered tissues.

1. Introduction

Marrow-derived mesenchymal stromal cells (MSCs) were first characterized for multipotency [1] with subsequent studies establishing a preference for osteogenic differentiation *in vitro* [2–4]. As a result, MSCs used in tissue engineering have historically been instructed to differentiate toward bone-forming osteoblasts. Based on limited evidence of transplanted MSCs differentiating to osteoblasts *in situ*, MSCs are more recently presumed to promote regeneration indirectly through secretion of trophic factors, such as vascular endothelial growth factor (VEGF) [5,6]. Strategies involving prolonged *in vitro* cultivation with sophisticated perfusion bioreactors result in excellent bone formation [7–9], but osteogenic progenitor cell populations cannot differentiate down an endothelial lineage. When applied for concomitant bone and vessel formation, numerous challenges have limited the potential efficacy of co-cultures of mesenchymal progenitors and endothelial cells, owing to incompatibilities in the soluble medium formulations. For example, both β-glycerophosphate and dexamethasone, widely used as osteogenic supplements, inhibit endothelial cell growth [10]. Thus, there is a critical need for successful approaches to harness the osteogenic potency of MSCs while promoting their ability to secrete angiogenic factors.

MSC-secreted VEGF declines as osteogenic differentiation progresses [11]. This suggests that a dual-instructive strategy is necessary

* Corresponding author. 451 Health Science Dr., 2303 GBSF, Davis, CA, 95616, USA.
E-mail address: jkleach@ucdavis.edu (J.K. Leach).
[1] These authors contributed equally.

https://doi.org/10.1016/j.biomaterials.2020.119973
Received 4 June 2019; Received in revised form 12 March 2020; Accepted 13 March 2020
Available online 20 March 2020
0142-9612/

to promote the simultaneous upregulation of proangiogenic factors with osteogenic differentiation of this heterogeneous population. Our group observed sustained osteogenic potential with increasing proangiogenic potential when osteogenically-induced MSCs engaged a complex, cell-secreted, decellularized extracellular matrix (ECM) [12]. We demonstrated that the ECM complexity is key for enhancing cell response, suggesting that multiple signaling pathways can be activated simultaneously in a single MSC population. This ECM could be used as a coating on implantable substrates [13–16], but limited opportunities exist for fabricating 3-dimensional materials derived from cell-secreted ECM for injection. The use of bioactive peptides offers an attractive alternative. Peptides are smaller and are thus more easily presented from a material, such as through covalent binding to alginate, without changing biomaterial properties. They also recapitulate many of the functions of matricellular proteins and offer improved stability [3,17,18].

The biophysical properties of alginate are highly tunable. Alginate's modulus is readily controlled by molar mass or crosslinker concentration [3,19], making it well-suited for leveraging substrate stiffness to modulate cell fate [3,20]. Recent studies have focused on the viscoelastic properties of biomaterials, which affect cellular proliferation, differentiation, and migration [21,22]. The extent of viscoelastic *versus* elastic properties can be controlled by crosslinker type: divalent ions such as calcium form reversibly breakable bonds and a primarily viscoelastic material, whereas covalent crosslinking, achieved in various manners such as carbodiimide chemistry, results in a purely elastic gel. These features give alginate another layer of tunability [21,22], which may facilitate the multi-modal signaling required to instruct an MSC population to build vascularized bone.

Here we investigate engineered alginate with two distinct instructive peptides and controlled biophysical properties to guide a population of human MSCs to (1) increase VEGF production and (2) simultaneously differentiate down the osteogenic lineage. As a corollary, we hypothesized that modulating the biophysical properties of the hydrogel would also influence the effect of the biochemical functionalization, underscoring the advantage of a single, tunable biomaterial engineered for multi-modal cell instruction.

2. Materials and methods

2.1. Peptide selection and synthesis

We selected three candidate peptides from the literature and tested their ability to promote network formation (1) when applied directly on human microvascular endothelial cells (hMVECs; Fig. 1 and 2) when applied on MSCs and the conditioned medium used to promote hMVEC network formation (Fig. 1). We sought to capture varying methods by which angiogenesis could be promoted: GHK (full sequence: KKGHK) is derived from osteonectin and has a wide array of functions in wound healing [18,23], QK (full sequence: KLTWQELYQLKYKGI) is a mimic of the VEGF receptor-binding region [23], and HepIII (full sequence: GEFYFDLRLKGDKYG) is a fragment of collagen IV, a component of the basement membrane that regulates invasion and formation of blood vessels [24].

Acetylated QK-amide (> 95% purity) was custom synthesized by GenScript (Piscataway, NJ). Peptide-acids were synthesized on glycine-Wang resin using standard Fmoc solid phase peptide synthesis on a CEM Liberty Blue automated microwave peptide synthesizer [23]. Briefly, Fmoc-glycine-Wang resin was swollen with dimethylformamide (DMF), then deprotected with 20% piperidine in DMF for 1 min at 90 °C before each amino acid coupling. Amino acids were coupled for 4–45 min each, depending on coupling optimization, at 90 °C using 5 equivalents each of Fmoc-amino acids, N,N′-diisopropylcarbodiimide (DIC), and OxymaPure with 0.1 M diisopropylethylamine (DIPEA). Peptides were cleaved for 3 h with 88% trifluoroacetic acid (TFA), 5% phenol, 5% water, and 2% triisopropylsilane (TIPS) and precipitated with cold diethyl ether. Crude peptides were redissolved in 5% acetonitrile and purified to > 90% purity through a C18 prep column against an acetonitrile gradient on an AKTApure 25 FPLC and confirmed by MALDI-TOF mass spectrometry.

2.2. Peptide screening

Synthesized peptides were dissolved at 30 μM in reduced growth factor endothelial growth medium (RGF), which consisted of EGM2-MV (Lonza) without VEGF, basic fibroblast growth factor (bFGF), and insulin-like growth factor (IGF). We confirmed previous observations [18] that omission of these three growth factors results in a medium that supports hMVEC viability but does not impart angiogenic signals (*data not shown*). hMVECs (Lonza, Walkersville, MD) were cultured on Matrigel (Corning, Corning, NY) in the RGF-peptide cocktail for 8 h prior to treatment with calcein (Invitrogen, Carlsbad, CA) for visualization of networks and fluorescent imaging. Fluorescent images were analyzed using AngioQuant [25] using threshold 15–255 and prune factor 25.

To assess the indirect effects of the peptides, we dissolved peptides at 30 μM in MSC expansion medium consisting of Dulbecco's Modified Eagle Medium (DMEM) with 4.5 g/L glucose (Thermo Fisher, Waltham, MA) supplemented with 100 U/mL penicillin and 100 μg/mL streptomycin (Cellgro, Manassas, VA), 10% v/v fetal bovine serum (FBS, Atlanta Biologicals, Flowery Branch, GA), and 2 mM L-glutamine (Thermo Fisher Scientific). Human MSCs (RoosterBio, Frederick, MD) were received at passage 2, and their trilineage potential was characterized by induction in lineage-specific media. MSCs at passage 4–5 were cultured in monolayer for 1 week in expansion medium with peptide. Medium with peptide was refreshed once during the culture duration [10]. At the end of the week, conditioned medium was collected and applied to hMVECs at a 1:3 ratio of conditioned medium to RGF. Culture, imaging, and analysis followed the same procedure as described above.

2.3. Peptide functionalization to alginate

We covalently modified VLVG alginate (50 kg/mol, G:M ratio > 1.5; Pronova, Sandvika, Norway) with QK, control QK peptide (CTRL QK; KVKFMDVYQRSYCHP; Genscript) [26], RGD (GGGGRGDSP; Peptide 2.0, Chantilly, VA), or RDG (GCRGYGRDGSPG; Genscript) as a scrambled peptide, using carbodiimide chemistry as we reported [3,18,27] with a degree of substitution (DS) of 10. Peptide conjugation was confirmed by NMR and quantified using a ninhydrin assay [3]. We created alginate solutions of varying QK:RGD content by mixing solutions of QK-alginate and RGD-alginate in different volume ratios. The alginate was dissolved at 25 mg/mL in either 2-(*N*-morpholino)ethanesulfonic acid (MES) buffer or phosphate buffered saline (PBS). The two buffers were used to accommodate the different crosslinking methods as detailed below. Unmodified alginate served as a negative control.

2.4. Formulation of viscoelastic and elastic alginate hydrogels

Viscoelastic gels were formed following a modified internal calcium carbonate gelation protocol [28]. Alginate in PBS was mixed with (1) $CaCO_3$ at 50 mg/mL and (2) glucono-δ-lactone (GDL; Sigma Aldrich, St. Louis, MO) at 150–200 mg/mL with a volume ratio of 8:1:1. The variation in GDL content controlled the amount of calcium ions liberated for crosslinking *via* lowering the pH, thereby varying the stiffness of the resulting gel. The mixture was pipetted into molds of 8 mm diameter and 1.5 mm height and allowed to gel at 37 °C for 3 h.

Elastic gels underwent carbodiimide covalent crosslinking as described previously [21]. Alginate in MES buffer was mixed with (1) 1-ethyl-3-(3-dimethylaminopropyl)carbodiimide (EDC; Sigma Aldrich) at 100 mg/mL and (2) a solution of adipic acid dihydrazide (AAD) and 1-

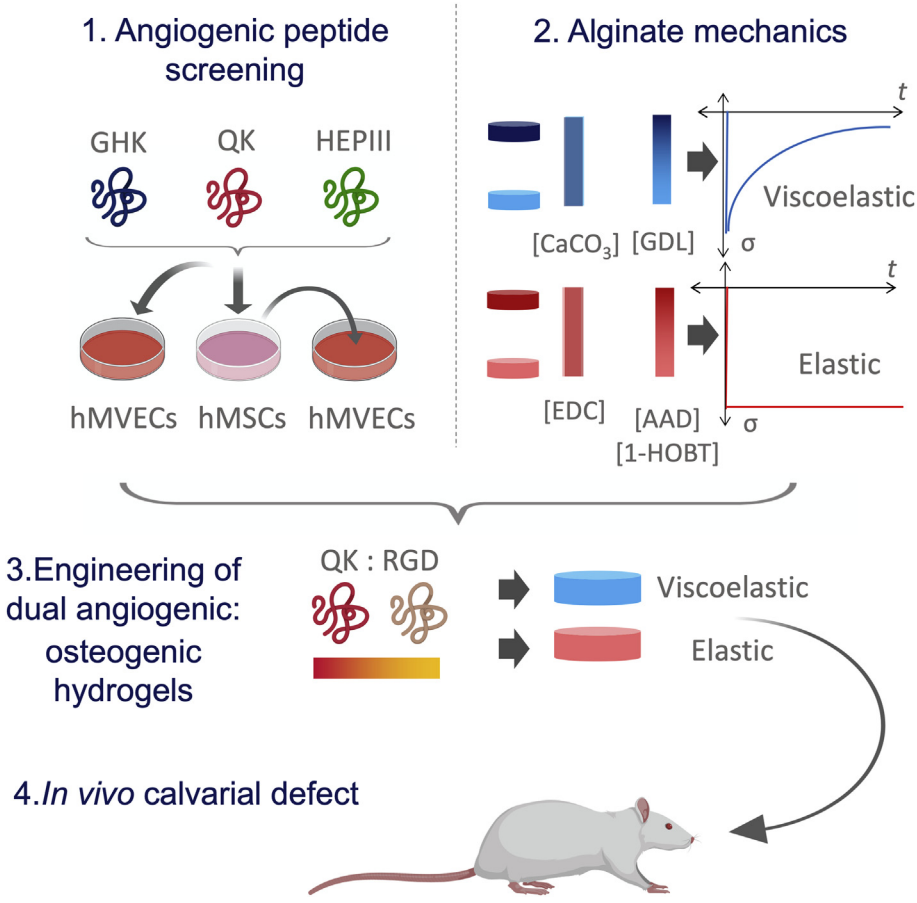

Fig. 1. Schematic of experimental workflow. 1) GHK, QK, and HepIII were applied in solution either directly to hMVECs or to MSCs to elicit production of conditioned medium, which was then applied to hMVECs. hMVEC network formation was assessed to select a peptide for further use. 2) In parallel, a library of viscoelastic or elastic alginate hydrogels were created with varying crosslinker concentrations to produce gels of varying moduli. 3) The effect of all combinations of peptide content, viscoelasticity, and stiffness on the ability of MSCs to promote hMVEC network formation and undergo osteogenic differentiation was assessed in a high-throughput experiment. 4) From this screen, one formulation was selected for *in vivo* studies.

hydroxybenzotriazole (1-HOBT; Sigma Aldrich), both at 25–75 mM. The mixture had a volume ratio of 8:1:1 alginate:EDC:AAD/1-HOBT. We controlled the number of crosslinks and resultant stiffness of the gel by variation in AAD content. The mixture was pipetted into identical molds as for viscoelastic hydrogels and allowed to gel under the same conditions. In both cases, the final concentration of alginate within the gels was 20 mg/mL.

2.5. Mechanical testing

Acellular and cell-containing gels were subjected to unconfined compression using an Instron 3345 (Instron, Norwood, MA) tester fitted with a 10 N load cell. For compressive stiffness, we applied a compressive deformation of 75 μm/s (5%/s) and determined the slope of the linear portion of the stress-strain curve. For stress relaxation tests, the ramp down was applied for 2 s and the deformation held constant for an additional 58 s. The stress *versus* time data from 2 s to 58 s was fit to a Maxwell stress relaxation model (Eqn. (1)):

$$\sigma = \sigma_0 e^{-\frac{t}{\tau}} + \sigma_e \quad (1)$$

where σ is normal stress along the axis of the gel disk, σ_0 is the initial stress due to the deformation by 2 s, t is time, τ is the time constant of relaxation, and σ_e is the stress at equilibrium by the end of the test. The time constant τ and the percentage of stress relaxed (f, Eqn. (2)) were used to characterize the stress relaxation behavior of the gel.

$$f = \left(\frac{\sigma_0 - \sigma_e}{\sigma_0}\right)100\% \quad (2)$$

2.6. Analysis of proangiogenic and osteogenic potential of MSCs entrapped in dual peptide alginate

We conducted a high-throughput study to test the ability of alginate gels of varying QK-RGD content, stiffness, and viscoelasticity to promote VEGF secretion and osteogenesis by entrapped MSCs. MSCs were encapsulated in all combinations of alginate formulations (Table 1) at 10^7 cells/mL, resulting in 48 groups with $n = 3$ per group. Constructs were cultured under expansion conditions for 1 week, when the conditioned medium was collected and applied to hMVECs on Matrigel. Network length, size, and number of junctions were quantified *via* AngioQuant and normalized to results from non-functionalized gels. Viability and metabolic activity of cells entrapped in viscoelastic and elastic gels were monitored by live/dead and alamarBlue assays, respectively.

We continued culture of the constructs in expansion medium supplemented with β-glycerophosphate (Sigma Aldrich) at 2 mM, a concentration that provides the MSCs with a phosphate source for mineralization but is insufficient for either dystrophic mineralization or a full osteoinductive signal [29]. This ensured that the biomaterial's effect on mineralization would be more readily apparent. At the end of the culture period, constructs were digested in passive lysis buffer for calcium and DNA quantification. Results from non-functionalized gels were subtracted from all other results to account for any signal due to the calcium used for crosslinking as opposed to biomineralization. The formulation balancing the highest levels of calcium per cell with the most robust hMVEC network formation response was chosen for subsequent studies.

2.7. Loss-of-function studies

In light of QK-mediated angiogenic potential, we probed the

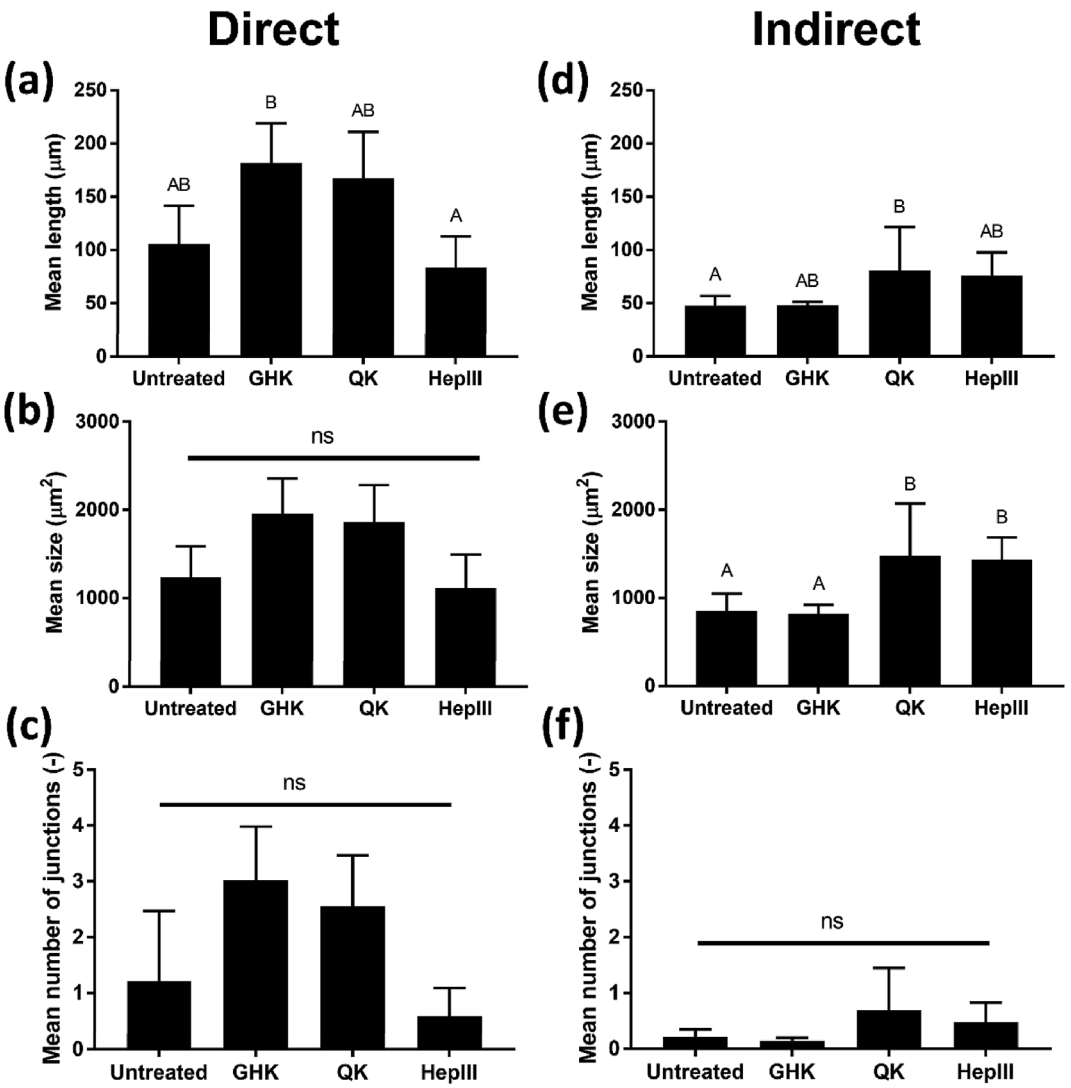

Fig. 2. Analysis of peptide stimulation of hMVEC network formation when applied directly to cells or when generating MSC conditioned medium for indirect hMVEC stimulation. When applied directly to hMVECs, both QK and GHK achieved significant increases in network length compared to HepIII, which performed similarly to the negative control (a). When conditioned media from stimulated MSCs was applied to hMVECs (indirect), QK and HepIII outperformed GHK in hMVEC network length and size (d–e). We did not detect significant differences in network branching in either mode (c, f). Representative images used to generate these data are shown in Supplementary Fig. S1a. Due to superior performance in both direct and indirect modes of action (n = 4), QK was chosen for all subsequent studies. Data points labeled with different letters are significantly different from one another at $p < 0.05$.

Table 1
List of all hydrogel compositions used in this study.

QK:RGD ratio	Crosslinker concentration	Gelation mode
0:1 1:3 1:1	150 mg/mL GDL or 25 mM AAD/1-HOBT 167 mg/mL GDL or 42 mM AAD/1-HOBT	Ionic ($CaCO_3$/GDL)
3:1 1:0 Untreated	183 mg/mL GDL or 58 mM AAD/1-HOBT 200 mg/mL GDL or 75 mM AAD/1-HOBT	Covalent (AAD/1-HOBT/EDC)

mechanism of QK signaling on MSCs. QK is designed to bind VEGF receptors, which MSCs do not express [30], yet VEGF can signal MSCs through platelet-derived growth factor (PDGF) receptors (PDGFRs) [31]. We conducted a loss-of-function study designed to inhibit three nodes in the PDGF signaling pathway. Anti-PDGFRβ antibody (25 μg/mL, R&D Systems, Minneapolis, MN; inhibits the entire pathway), wortmannin (5 ng/mL, Sigma Aldrich; inhibits phosphoinositide 3-kinase (PI3K)), and Ruxolitinib (5 nM, Sigma Aldrich; inhibits Janus kinases (JAK) 1 and 2) were applied to viscoelastic constructs containing 1:1 QK-RGD and 10^7 cells/mL for 1 week. An untreated elastic group served as a negative control. We quantified VEGF in the conditioned media *via* enzyme-linked immunosorbent assay (ELISA) kit (R&D Systems) and normalized VEGF concentrations to total cell number using the Quant-iT PicoGreen dsDNA Assay Kit (Thermo Fisher).

2.8. Rat calvarial defect studies

Treatment of experimental animals was in accordance with UC Davis animal care guidelines and all National Institutes of Health animal handling procedures. Viscoelastic and elastic hydrogels were equilibrated in growth medium overnight prior to implantation into a rat bilateral calvarial defect as previously described [32,33]. Briefly, male 12-week-old nude rats (Taconic Biosciences, Germantown, NY) were anesthetized (3.0%) and maintained (1.5%) under an isoflurane/O_2 mixture delivered through a nose cone at 6 L/min. As this study was designed to test the dual potential of MSCs, only male rats were used due to inferior vascularization observed with MSC-loaded constructs

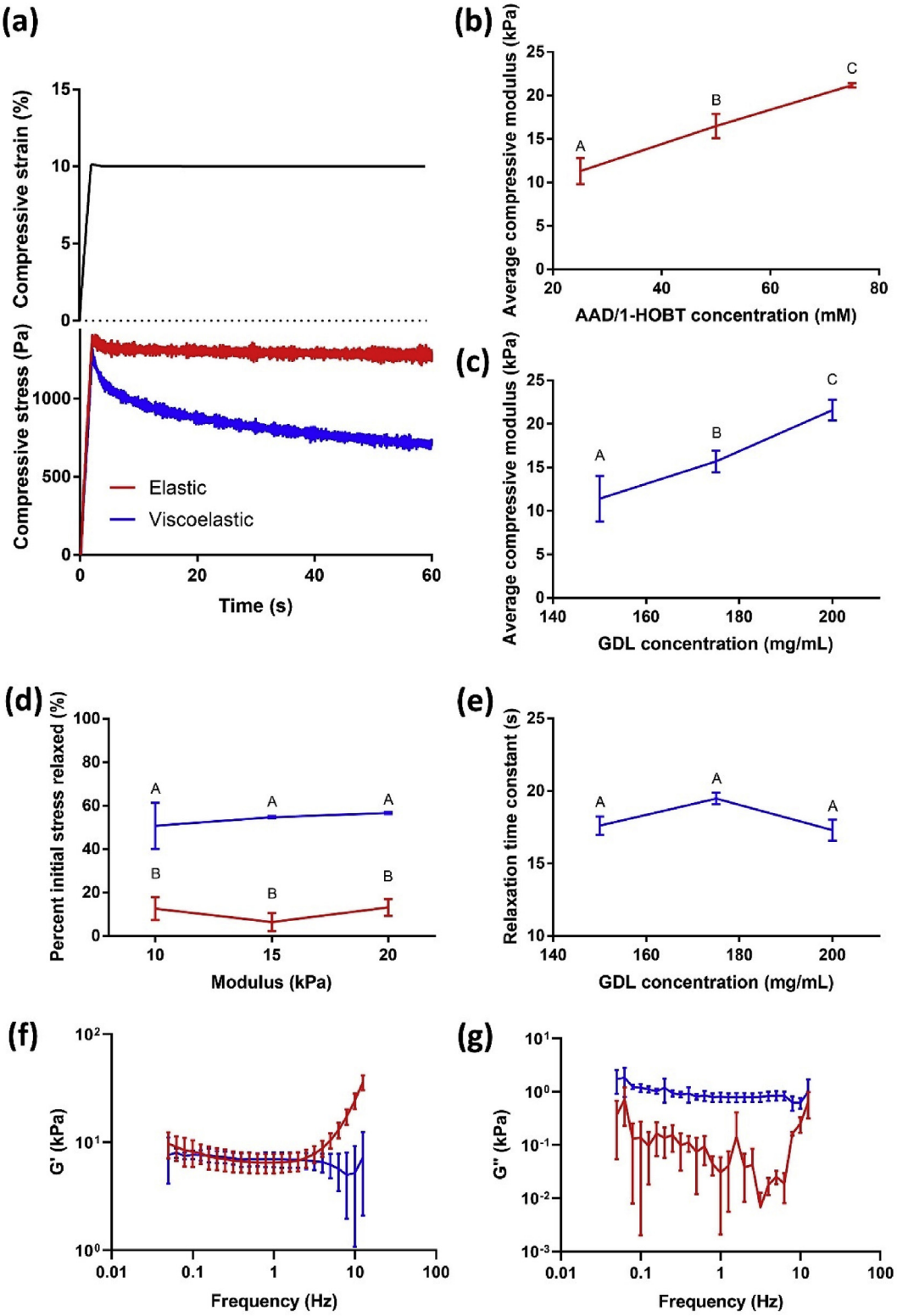

Fig. 3. Development of a mechanical library of alginate hydrogels. Representative strain and stress curves *versus* time of AAD/HOBT-crosslinked elastic gels (red) or GDL-crosslinked viscoelastic gels (blue) (a). Changing the concentration of either AAD and 1-HOBT for elastic gels (b) or GDL for viscoelastic gels (c) resulted in similar stiffness between 10 and 20 kPa. Ionically crosslinked gels exhibited significant stress relaxation (viscoelastic behavior), while the stress remained relatively constant for covalently crosslinked gels (d) consistent with elastic material behavior. The time constant of relaxation in the viscoelastic gels did not change with crosslinker concentration (e), (n = 3). A frequency sweep of elastic and viscoelastic gels resulted in similar storage moduli (f), but a loss modulus was only detected in viscoelastic gels (g). Data points labeled with different letters are significantly different from one another at $p < 0.05$. (For interpretation of the references to color in this figure legend, the reader is referred to the Web version of this article.)

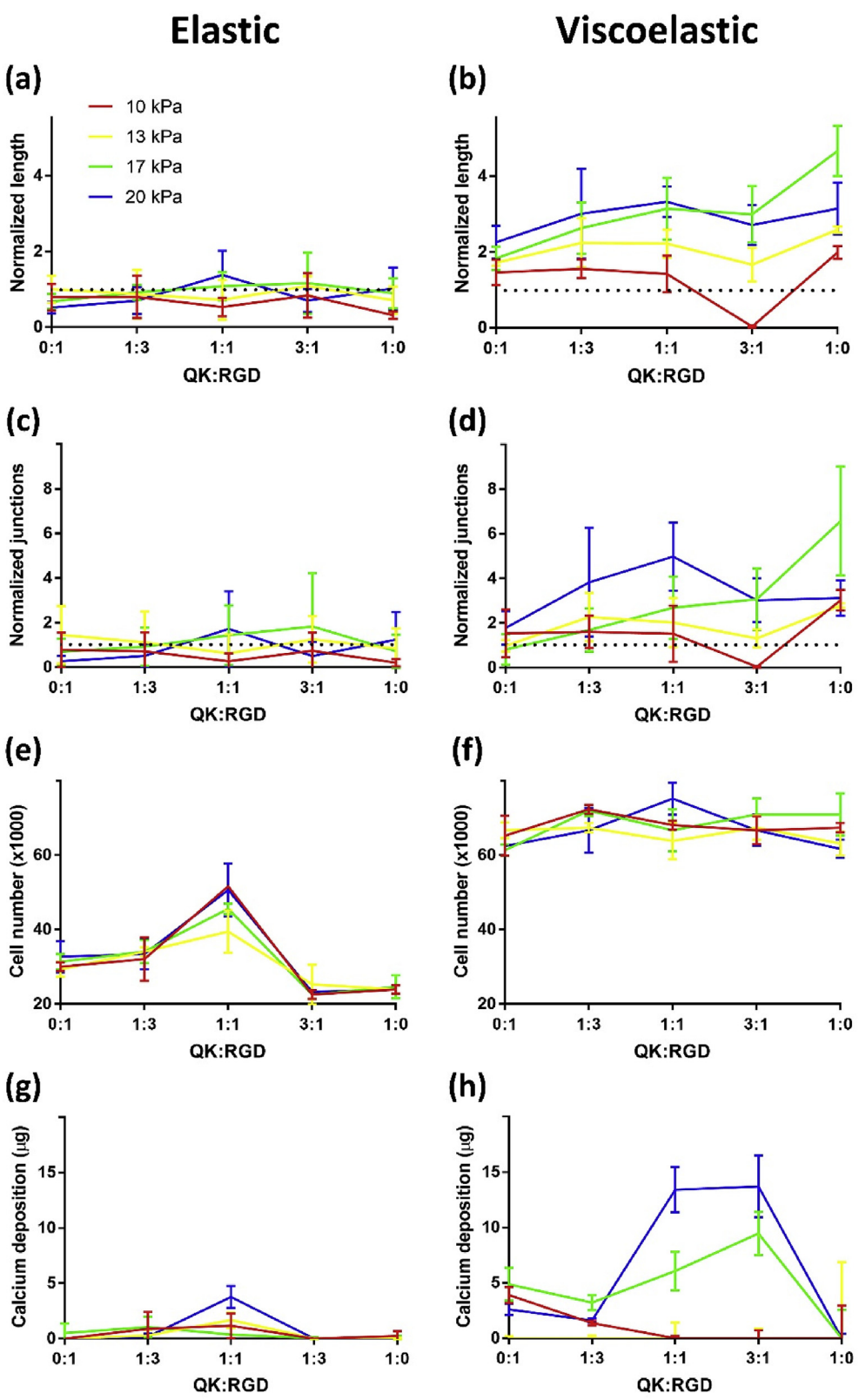

Fig. 4. Viscoelastic gels with 1:1 QK:RGD content and high stiffness promote the most indirect angiogenesis and direct osteogenesis. MSCs cultured in alginate gels of varying QK:RGD content (*x*-axes), stiffness (colored lines), and viscoelasticity (left *versus* right) exhibited differences in ability of conditioned medium to elicit hMVEC network formation, proliferation, and calcium deposition. Viscoelastic gels outperformed elastic gels in all outputs tested, with 17–20 kPa gels containing 1:1 or greater QK:RGD achieving the highest indirect network formation and direct proliferation/total calcium content (n = 3). Representative images used to generate these data are shown in Supplementary Fig. S1b.

when implanted into female rats [8]. A mid-longitudinal 15 mm skin incision was made on the dorsal surface of the cranium. The periosteum was completely cleared from the surface of the cranial bone by scraping. A trephine bur was used to create one circular 3.5 mm diameter defect in the rat cranium on each side of the sagittal suture, and the full thickness (~1 mm) of the cranial bone was removed. 20 kPa viscoelastic and elastic gels functionalized with 1:1 QK:RGD and containing 10^7 cells/mL were generated with a final diameter of 3.5 mm and placed directly into the osteotomy site. Empty defects served as a negative control. Animals were euthanized at 2- or 12-weeks post-implantation, and calvariae were harvested, fixed in 4% w/v formalin and kept in 70% v/v ethanol until further processing.

Blood flow was measured on anesthetized animals using a Periscan PIM 3 laser Doppler perfusion imager (LDPI; Perimed, Stockholm,

Sweden). The hair covering the surgical site was removed the day before scanning, and the skin was cleaned using alcohol wipes immediately prior to data acquisition. Perfusion measurements were obtained from a circular region of interest superimposed over the defect.

Microcomputed tomography (microCT) scans were performed using a high-resolution microCT specimen scanner (mCT 35; Scanco Medical, Brüttisellen, Switzerland) with a 70 kVp X-ray source at 114 μA and 300 ms integration time. Quantification was performed by setting a threshold of 256–3000 mg HA per cm^3 to discriminate between mineralized and unmineralized tissue. After thresholding, the image noise was reduced using a low pass Gaussian filter ($\sigma = 0.8$, support = 1). Reconstructed 3D images were generated from the scans and used to visualize mineral distribution throughout the constructs. Bone volume fraction (BV/TV) was determined by dividing the number of pixels representing bone tissue (BV: bone volume) by the number of pixels in the cylindrical segment (TV: total volume).

After microCT analysis, the samples were demineralized in Calciclear (National Diagnostics, Atlanta, GA) for 7 days, dehydrated in a graded series of ethanol baths, embedded in paraffin wax, sectioned at 10 μm, and affixed to microscope slides. The sections were stained with H&E and Masson's trichrome to assess bone formation. To assess osteogenic differentiation and vascular invasion, sections were stained with a primary antibody against osteocalcin (1:1000, AB13420, Abcam, Cambridge, MA) and von Willebrand factor (vWF) (1:200, AB6994, Abcam). The presence of vascular structures was quantified by counting distinct areas of vWF staining by two blinded reviewers.

2.9. Statistical analysis

Data are presented as means ± standard deviation unless otherwise stated. Except in Fig. 4, statistical analysis utilized a one-way ANOVA with post-hoc Tukey test. $p < 0.05$ was considered significant. In Fig. 4, we employed a three-way ANOVA with post-hoc Tukey test. In each graph, data points with different letters are significantly different from one another.

3. Results

3.1. Peptide screen

When stimulating cells directly with peptides in the media, hMVECs exhibited greater average network length when exposed to GHK and QK (Fig. 2, **left**). In contrast, MSCs treated with QK and HepIII produced conditioned media that elicited the highest average hMVEC network length and size (Fig. 2, **right**). We detected no significant difference in the mean number of junctions within the hMVEC networks regardless of peptide or mode of stimulation (Fig. 2c and f, and Supplementary Fig. 1a). Due to its ability to promote network formation in both direct and indirect modes, we selected QK for all subsequent studies.

3.2. Alginate mechanics

The different modes of crosslinking had a dramatic effect on the stress relaxation characteristics of the resulting gel (Fig. 3a). Viscoelastic gels produced by ionic crosslinking exhibited ~60% relaxation of the initial stress (Fig. 3d). Aside from an initial slight decrease in stress, which we attributed to an observable initial decrease in strain due to the transition between ramp-down and hold, elastic gels formed by covalent crosslinking exhibited constant stress at constant strain. We could influence the average compressive modulus of hydrogels by changing the concentration of AAD/1-HOBT for elastic gels or GDL for viscoelastic gels. Specifically, 25–75 mM AAD/1-HOBT and 150–200 mg/mL GDL resulted in gels of comparable stiffness, possessing moduli of 10–20 kPa (Fig. 3b–c). Storage moduli between elastic and viscoelastic gels were similar as evidenced by a frequency sweep from 0.05 to 10 Hz (Fig. 3f), but strain energy dissipation only occurred in viscoelastic gels (Fig. 3g). Cell-laden viscoelastic gels (14.4 ± 1.0 s, n = 3) exhibited a slight decrease in stress relaxation time compared to acellular viscoelastic gels (17.9 ± 1.7 s, n = 4; $p = 0.023$), suggesting that cells interfere with the crosslinking process. Interestingly, GDL concentration had no effect on the relaxation time constant of viscoelastic gels (Fig. 3e). We observed comparable efficiencies of peptide modification, yielding polymers with a DS of approximately 10 for both peptides.

3.3. Gel screen

We used Matrigel network formation induced by conditioned media, MSC proliferation, and MSC calcium deposition as outputs in the high-throughput experiment to determine the effect of relative peptide concentration and mechanics on MSC promotion of angiogenesis and MSC osteogenesis. In general, viscoelastic gels exhibited superior results compared to elastic gels in all outputs assessed (Fig. 4). MSCs in elastic gels, regardless of stiffness or peptide composition, did not produce conditioned medium significantly more angiogenic than non-functionalized controls. In contrast, MSCs in viscoelastic gels had noticeable differences, with increasing stiffness and QK-RGD ratio corresponding with increased network length and number of junctions (Supplementary Fig. 1b). Mean network area followed the same trend as did network length (*data not shown*).

At the end of the three-week culture, MSCs in elastic gels exhibited the greatest cell number at the 1:1 QK:RGD ratio (Fig. 4e). In contrast, we did not detect differences in MSC number within viscoelastic gels as a function of peptide ratio, yet MSC number was greater than in elastic gels. MSCs in viscoelastic gels also produced more calcium compared to cells in elastic gels except at (1) low stiffnesses and (2) high QK-RGD ratios. At 1:1 and 3:1 QK:RGD, both 17 and 20 kPa ionic gels induced markedly increased calcification. The 1:1 QK:RGD, 20 kPa, viscoelastic gels were the most significantly different from the other groups (Supplementary Table S1). Compared to viscoelastic gels, we observed a reduction in cell viability and metabolic activity after 1 day in elastic gels (*data not shown*). However, DNA content was similar after 2 weeks in culture, suggesting that the cytotoxicity of chemicals used to crosslink covalent gels was transient. While 100% QK gels performed better in the angiogenesis assays, their lack of calcium deposition prompted the selection of 1:1 QK:RGD, 20 kPa for all subsequent studies.

To confirm that the observed effects on MSC behavior in the 1:1 QK:RGD 20 kPa viscoelastic gels were due to the specific peptides presented from the alginate backbone, we assessed the effects of unmodified and control peptide-functionalized elastic and viscoelastic hydrogels. The RDG peptide was chosen as scrambled peptide to RGD, while a control QK (CTRL QK) peptide, corresponding to the unmodified 14–28 region of QK which lacks secondary structure required for receptor interaction and does not bind to VEGFR [26], served as control for the QK peptide. 20 kPa elastic and viscoelastic unmodified alginate gels and peptide-functionalized gels containing a 1:1 ratio of either CTRL QK:RDG, CTRL QK:RGD, QK:RDG or QK:RGD were cultured *in vitro* for 7 days, when the conditioned media was collected and used to stimulate the network formation of hMVECs (Supplementary Fig. 2). Conditioned media from QK:RDG and QK:RGD viscoelastic gels induced greater hMVEC network formation, evidenced by endothelial networks with increased mean length (Supplementary Fig. 2a and b), size (Supplementary Fig. 2c and d) and number of junctions (Supplementary Fig. 2e and f). After collection of the conditioned media, hydrogels were further cultured to induce osteogenic differentiation of encapsulated MSCs. We observed increased calcium deposition in viscoelastic QK:RGD- and CTRL QK:RGD- functionalized gels compared to all other groups (Supplementary Fig. 3a and b), and these data were supported by histological analysis of calcium deposition (Supplementary Fig. 3c). H&E staining revealed a more spindle-like cellular morphology of cells in viscoelastic RGD-modified gels (Supplementary Fig. 3d), confirming the interaction of the encapsulated

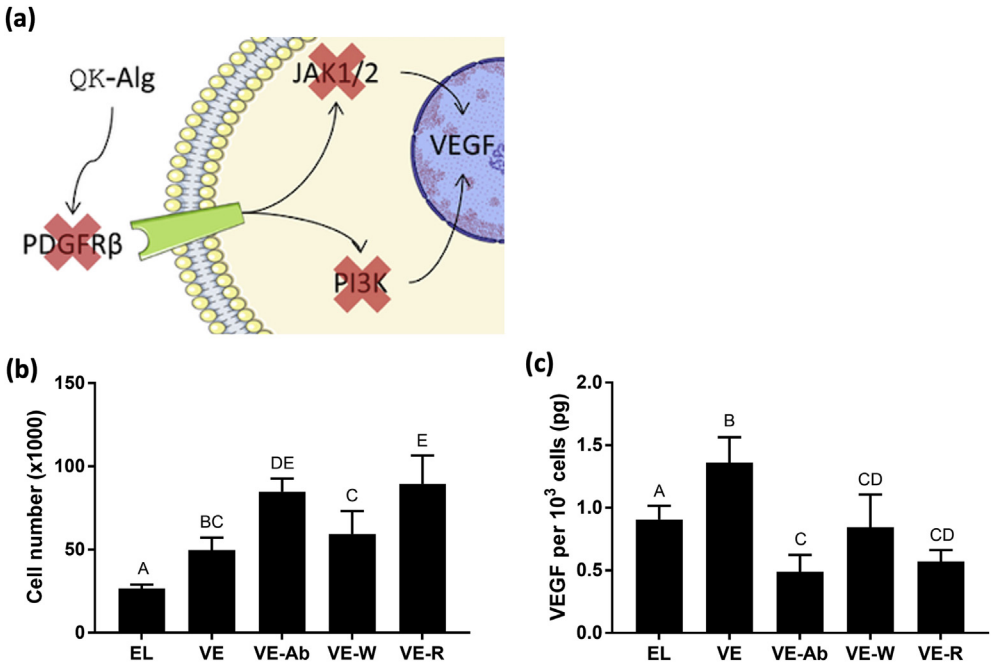

Fig. 5. QK exerts its effects through the PDGF receptor. (a) Schematic of mechanistic studies to interrogate QK signaling pathways. Anti-PDGFRβ (inhibits PDGFRβ binding), wortmannin (inhibits PI3K), and Ruxolitinib (inhibits JAK1/2) were applied to MSCs in 20 kPa ionic gels with 1:1 QK:RGD (VE-Ab, VE-W, and VE-R, respectively) for 7 days. Untreated elastic (EL) and viscoelastic (VE) gels with the same stiffness and peptide content served as controls. (b) Cell number within 1:1 QK:RGD gels (n = 4). (c) Quantification of VEGF secretion by entrapped MSCs in 20 kPa viscoelastic gels with 1:1 QK:RGD in presence of inhibitors (n = 4). Data points labeled with different letters are significantly different from one another at $p < 0.05$.

MSCs with the RGD peptide on the alginate backbone. In contrast, MSCs in RDG-modified gels and the covalent gels exhibited a rounded morphology.

3.4. Loss-of-function mechanistic studies

MSCs encapsulated in 1:1 QK:RGD, 20 kPa viscoelastic gels exhibited significant differences in both cell number and VEGF secretion per cell when exposed to various inhibitors of the PDGFRβ signaling cascade (Fig. 5a). Inhibition of the PDGF receptor and JAK1/2 had the greatest effect, increasing cell number and decreasing VEGF secretion (Fig. 5b–c). Notably, inhibition of the receptor decreased VEGF levels below those from elastic gels with the same peptide content and stiffness. Inhibition of PI3K had a smaller, but still significant, inhibitory effect on VEGF secretion.

3.5. Angiogenesis and osteogenesis in vivo

Two weeks after implantation, we observed cell infiltration and vascularization in defects treated with MSC-containing QK:RGD elastic and viscoelastic hydrogels through macroscopic examination, H&E, and vWF staining (Fig. 6a–c). We quantified greater blood vessel density in defects treated with MSC-containing gels compared to the empty control ($p = 0.032$ for elastic gels and $p = 0.019$ for viscoelastic gels, respectively). H&E staining revealed the presence of alginate in both experimental groups (Fig. 6b), with elastic gels exhibiting a significantly thicker tissue inside the defect (Fig. 6f) compared to the empty control ($p = 0.042$), suggesting faster alginate degradation in viscoelastic gels. The osteogenic potential of the implants was confirmed by osteocalcin immunostaining. Compared to elastic gels that exhibited limited cell infiltration and new tissue formation, we detected more intense osteocalcin staining in defects treated with viscoelastic gels, specifically located in the non-degraded alginate deposits (Fig. 6d). Perfusion within the defect site was noninvasively evaluated using laser Doppler perfusion imaging (Fig. 6g–h). Although treated defects exhibited similar perfusion through 2 weeks after implantation, in agreement with histological characterization of vascularization, perfusion within defects treated with viscoelastic gels continued to increase until week 4, while defects treated with elastic gels peaked at week 3 and began to decline.

MicroCT analysis of the defect area (Fig. 7a–b) revealed significant increases in bone volume fraction ($p = 0.022$) (Fig. 7f) and average mineral density ($p = 0.0162$) (Fig. 7g) in defects treated with viscoelastic gels compared to empty controls. Defects treated with elastic gels exhibited higher indices of bone formation than empty controls, on average, yet they were not significantly different ($p = 0.273$ for bone volume fraction; $p = 0.2043$ for average mineral density). H&E and Masson's trichrome staining also demonstrated areas of new bone formation in defects treated with both elastic and viscoelastic gels (Fig. 7c–d), with osteoid regions rich in disorganized collagen apparent. We also observed the presence of alginate in defects treated with elastic gels but not viscoelastic gels (Fig. 7c–d), suggesting slower degradation of elastic gels. We detected increased osteocalcin immunostaining within viscoelastic gels compared to elastic gels (Fig. 7e).

4. Discussion

When used in a cell-based therapy, MSCs are commonly delivered by direct injection with no supporting biomaterial or differentiation-instructive signals, relying mostly on their regenerative secretome rather than on differentiation. In this study, we capitalized on the high tunability of alginate to direct two different modes of MSC action – paracrine promotion of angiogenesis *via* trophic factor secretion and direct osteogenic differentiation. A key finding in this work is the confirmation of our sub-hypothesis: variation in biophysical properties modulates the effect of peptide functionalization *in vitro* and *in vivo*. Both elastic and viscoelastic gels contained the same peptides at the same concentrations, yet MSCs were more responsive to these peptides when presented in viscoelastic gels as evidenced by the dramatic increases in both angiogenic and osteogenic potential *in vitro* and improved bone formation *in vivo*. As such, this study uniquely harnesses the synergy between biochemical and biomechanical functionalization of alginate to instruct MSCs.

As the method of peptide functionalization utilized here – carbodiimide chemistry – does not depend on the peptide itself, we conducted an initial screen to identify the best peptide for our objective. We examined the responsiveness of cells in monolayer to free peptides for simplicity, as our goal was to screen peptides rather than investigate their action in detail. While our previous work on GHK-modified hydrogels successfully signaled MSCs to upregulate VEGF production

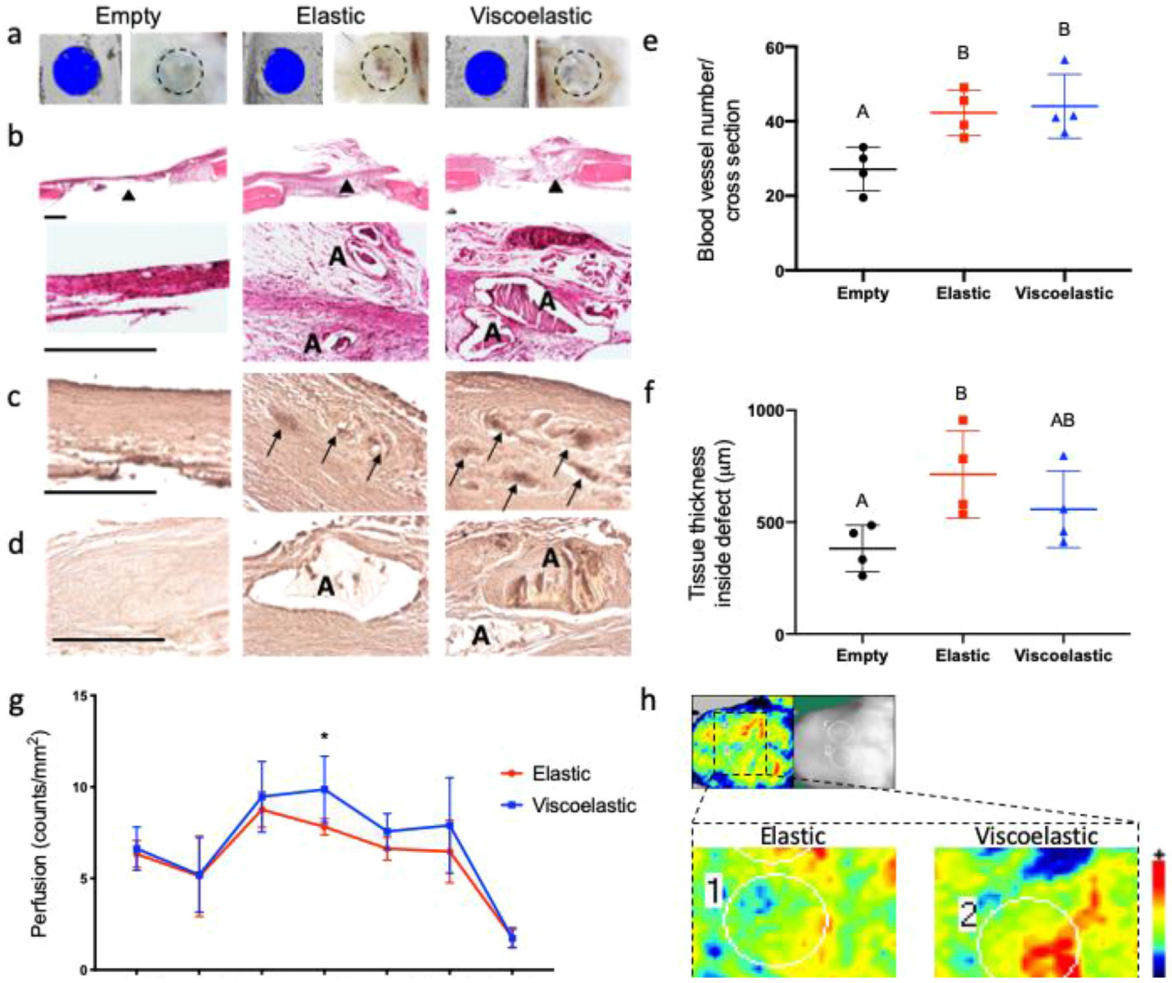

Fig. 6. Analysis of early vascularization and osteogenic potential in QK:RGD functionalized elastic and viscoelastic hydrogels after 2 weeks of *in vivo* implantation. (a) microCT and macroscopic images of the control empty defects or defects filled with either viscoelastic or elastic hydrogels. Histologic sections stained with (b) H&E, (c) von Willebrand factor and (d) osteocalcin. Quantification of (e) blood vessel density ($p = 0.019$ between the empty and the viscoelastic groups, $p = 0.032$ between the empty and the elastic group and $p = 0.933$ between the elastic and the viscoelastic groups) and (f) tissue thickness inside the defect ($p = 0.32$ between the empty and the viscoelastic groups, $p = 0.042$ between the empty and the elastic group and $p = 0.396$ between the elastic and the viscoelastic groups) (n = 4). (g) Quantification of blood perfusion at the defect area from laser Doppler perfusion imaging (LDPI). Statistical significance of $p < 0.05$ between the groups at the same time point is denoted by one asterisk (n = 5). (h) LDPI representative images of the covalent and ionic implantation areas at week 4. Black triangles denote the area where the 20x magnification picture was taken, "A" denotes the presence of residual alginate and the black arrows denote positively stained areas of blood vessel activity. Scale bars represent 500 μm for B and 250 μm for C and D.

[18], the free GHK peptide was ineffective in indirectly stimulating angiogenesis in these studies. The discrepancy in presentation between substrate-bound and free peptides may account for this, as peptides bound to a substrate may exert enhanced effects [34], representing a potential limitation of our study. GHK may still be a viable candidate for indirect angiogenesis when substrate-bound, but its bioactivity appeared blunted in the free form. Interestingly, our data also showed that HepIII was more effective in indirect than direct angiogenesis. Regardless, QK performed well in both direct and indirect assays, supporting its use in the subsequent studies investigating direct and indirect stimulation of angiogenesis.

Although the focus of this study was on the ability of the peptide to promote angiogenesis indirectly by promoting trophic factor secretion by MSCs, we also assessed the direct effect of the peptides on hMVECs to explore a potential secondary function on resident endothelial cells migrating into the construct post-implantation. From this perspective, the observed angiogenic efficacy of QK on hMVECs was expected and supported by literature, as QK mimics the receptor-binding region of VEGF [23,35]. While MSCs do not express VEGF receptors [30], they can respond to VEGF *via* activation of PDGFRs [31]. This upregulates VEGF secretion [36–38] *via* NF-κB translocation into the nucleus through the PI3k-Akt pathway [39] or STAT3 nuclear translocation *via* JAK1 activation [40]. Taken together, we hypothesized that QK was acting on MSCs by upregulating VEGF production *via* one or both of these pathways downstream of PDGFR activation in our system. We specifically focused on neutralizing PDGFRβ due to its higher affinity for PDGF-BB, a factor well-established to have an important role in mediating MSC support of angiogenesis [41]. As a result, QK could still influence MSCs *via* dimerized PDGFRα in our loss-of-function study. Despite this, antibody neutralization of PDGFRβ resulted in dramatic decreases in VEGF secretion per cell. We observed a similar drop with inhibition of the JAK-STAT pathway but not with inhibition of the PI3K pathway. Interestingly, in the groups with decreased VEGF production, proliferation was greatly increased. This suggests that QK may be exerting the mitogenic effects of PDGFR activation primarily through PDGFRα and pro-angiogenic effects, such as increased VEGF production, through PDGFRβ. As a detailed mechanistic study is outside the scope of the current study, these data will inform future studies on the biochemical events within MSCs when exposed to QK and on the secretome of MSCs in response to QK.

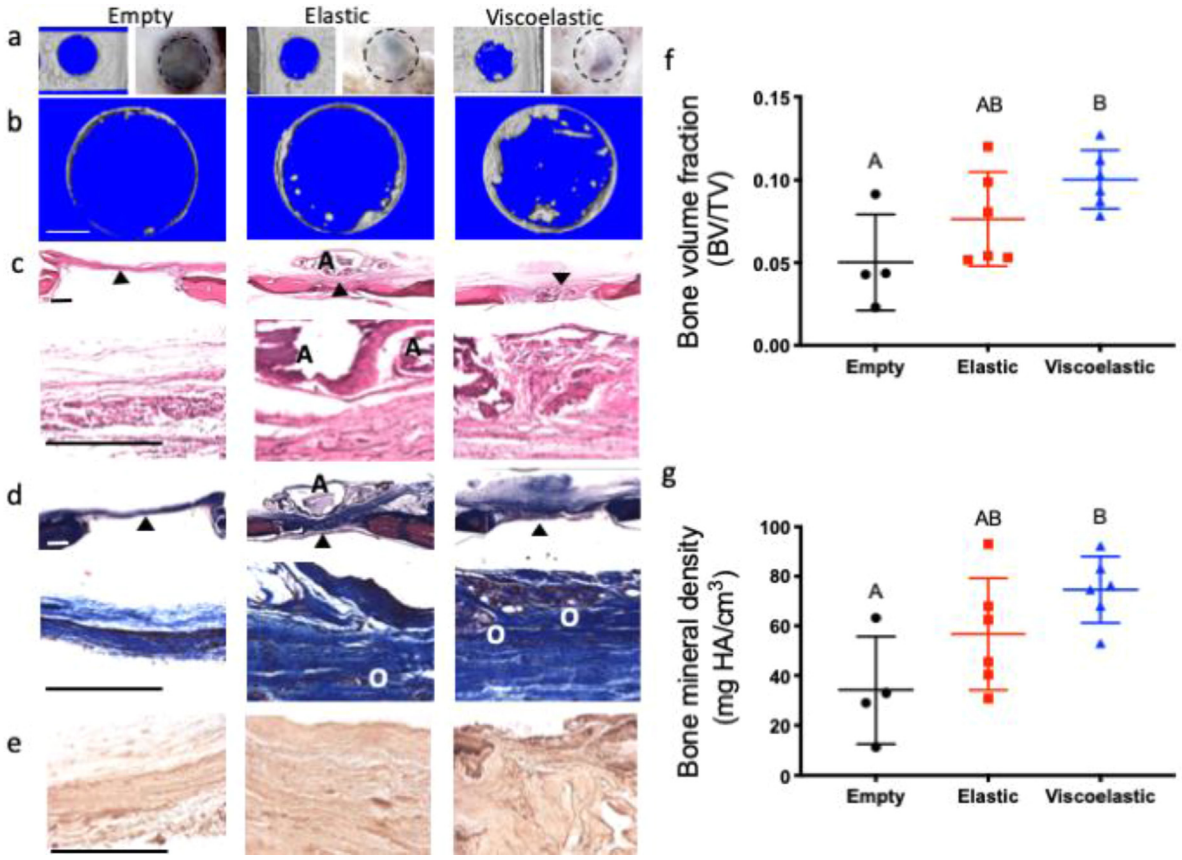

Fig. 7. Analysis of bone formation in QK:RGD functionalized elastic and viscoelastic hydrogels after 12 weeks. (a) microCT and macroscopic images of the control empty defects or defects transplanted with either elastic or viscoelastic hydrogels. (b) Area of microCT analysis to determine bone volume and mineral density in the defects. Histologic sections stained with (c) H&E, (d) Masson's trichrome and (e) osteocalcin. Quantification of (f) bone volume fraction ($p = 0.022$ between the empty and the viscoelastic groups, $p = 0.273$ between the empty and the elastic group and $p = 0.261$ between the elastic and the viscoelastic groups) and (g) average bone mineral density ($p = 0.016$ between the empty and the viscoelastic groups, $p = 0.204$ between the empty and the elastic group and $p = 0.276$ between the elastic and the viscoelastic groups) (n = 4 for the empty control, n = 6 for the elastic and viscoelastic groups). Black triangles denote the area where the 20x magnification picture was taken, "A" denotes the presence of residual alginate and "O" denotes areas of osteoid formation. Scale bars represent 1 mm for (b), 500 μm for (c) and (d), and 250 μm for (e).

While we used QK to promote the proangiogenic function of MSCs, we used hydrogel mechanics to drive their osteogenic differentiation. The chemicals used for covalent crosslinking of the elastic gels have been reported as cytotoxic [21,42]. Indeed, we observed a reduction in cell viability after 24 h. However, DNA content was comparable across all groups after 2 weeks in culture, suggesting that the detrimental effect of these chemical was transient. This finding suggests alternative methods to prepare elastic gels are merited to further characterize the effect of gel mechanics on cell differentiation stimulated by multiple peptides. In this study, MSCs were never exposed to full osteogenic medium, and thus, they were dependent upon the material to differentiate. MSCs in elastic gels exhibited little to no osteogenic differentiation, even in groups with high concentrations of RGD and high stiffness, two factors that generally enhance osteogenesis [17,20]. In contrast, MSCs in viscoelastic gels attained markedly increased calcification in higher stiffness gels. Interestingly, we observed low calcium content in 100% RGD gels. A 1:1 or 3:1 QK:RGD ratio promoted the most mineralization. This is unlikely due to any osteogenic effect of QK for a variety of reasons: (1) gels with 100% QK exhibited no osteogenesis regardless of stiffness; (2) gels with increased calcium content generally also showed increased proliferation, suggesting that MSCs were not being driven down the osteogenic lineage on a per-cell basis; and (3) PDGF signaling does not enhance MSC osteogenesis [43]. It is more likely that a viscoelastic substrate, coupled with sufficient RGD ligands for cell adhesion, along with the mitogenic effects of QK-PDGFR signaling, enhanced MSC proliferation and thereby increased total mineral content.

We characterized the stiffness of the viscoelastic gels in a manner similar to our characterization of elastic gels by using the slope of the stress-strain curve resulting from a linear ramp-down. This is a simplification of viscoelastic materials, which exhibit strain-rate dependency. Though this method has been used before to quantify stiffness of viscoelastic gels [22], it represents a limitation of the current work, resulting in difficulties comparing the defined 10–20 kPa elastic gels *versus* the viscoelastic gels. Nevertheless, characterization of storage moduli by frequency sweep rheometry revealed similar storage of strain energy between elastic and viscoelastic gels, supporting the comparison used in this study. A more detailed study focusing on the strain rates applied by resident cells in both elastic and viscoelastic substrates would better define the mechanical microenvironment experienced by the cells themselves, allowing for a more relevant quantification of modulus. In this work, the ability of viscoelastic gels to outperform elastic gels is clear, as is the enhancement of proangiogenic and osteogenic functions at higher stiffnesses in viscoelastic gels. Both of these observations support the initial hypothesis of the study.

The viscoelastic and elastic gels performed differently *in vivo* with respect to both angiogenesis and osteogenesis. Initial increases in vessel infiltration 2 weeks after implantation were similar in defects treated with MSC-containing gels but significantly higher than untreated defects. In addition, LDPI analysis of *in vivo* vascularization revealed similar perfusion levels between both groups until week 3, with vascularization continuing to increase in defects treated with only the

viscoelastic gels. These data suggest the viscoelastic gels enhanced the proangiogenic activity of entrapped MSCs compared to their elastic counterparts despite identical peptide content, which was in agreement with our *in vitro* results. Furthermore, after 2 weeks of implantation, we observed more intense osteocalcin staining localized in the viscoelastic alginate deposits, suggesting a direct contribution of the encapsulated MSCs on *de novo* bone formation. At week 12, viscoelastic gels produced more mineralized tissue per unit volume, an observation supported by visible differences in staining for both collagenous matrix and osteocalcin. While stress relaxation was the main difference between the groups studied here, we also observed differences in the relative rate of degradation. We detected no residual alginate in defects treated with viscoelastic gels, yet defects treated with elastic gels contained remnants of the material at 12 weeks. This suggests that faster degradation of viscoelastic gels may represent an additional mechanism for increased angiogenesis and osteogenesis *in vivo*, thereby facilitating tissue infiltration and growth. These data are in agreement with other studies reporting that alginate gels undergoing faster stress relaxation resulted in accelerated bone formation, cell infiltration, extensive matrix remodeling, and hydrogel disappearance within a rat calvarial defect compared to slow-relaxing hydrogels [44]. Similarly, bone formation was markedly increased when MSCs were transplanted in alginate that had been oxidized to enable hydrolysis compared to non-oxidized gels [45]. The design of these studies prevents our determination of whether bone formation was due to degradation of the hydrogel or viscoelasticity, representing a limitation of these studies and an area of future investigation.

Importantly, the MSCs implanted into the rat calvarial defects were not preconditioned for any lineage. The orthotopic site contains osteoinductive factors, but these were insufficient for noticeable healing as evidenced by the low mineral and vessel content in the empty controls. The higher levels of regeneration achieved by the viscoelastic constructs by virtue of material properties alone is notable in this regard and reveals new possibilities for combination with other clinically relevant pro-regenerative strategies such as cellular aggregation into spheroids [46], lineage-specific preconditioning [3], or hypoxic preconditioning [47].

5. Data availability statement

The raw/processed data required to reproduce these findings will be made available on request.

CRediT authorship contribution statement

Ben P. Hung: Conceptualization, Methodology, Validation, Formal analysis, Investigation, Writing - original draft, Writing - review & editing, Visualization. **Tomas Gonzalez-Fernandez:** Conceptualization, Methodology, Validation, Formal analysis, Investigation, Writing - original draft, Writing - review & editing, Visualization. **Jenny B. Lin:** Methodology, Investigation. **Takeyah Campbell:** Investigation, Writing - review & editing, Visualization. **Yu Bin Lee:** Conceptualization, Investigation. **Alyssa Panitch:** Conceptualization, Methodology, Formal analysis, Writing - original draft, Writing - review & editing. **Eben Alsberg:** Conceptualization, Methodology, Formal analysis, Writing - original draft, Writing - review & editing. **J. Kent Leach:** Conceptualization, Methodology, Formal analysis, Writing - original draft, Writing - review & editing, Supervision, Project administration, Funding acquisition.

Declaration of competing interest

The authors declare that they have no known competing financial interests or personal relationships that could have appeared to influence the work reported in this paper.

Acknowledgments

Research reported in this publication was supported by the National Institute of Dental and Craniofacial Research of the National Institutes of Health under award numbers R01 DE025899 and R01 DE025475 to JKL. TGF was supported by an American Heart Association Postdoctoral Fellowship (19POST34460034). The content is solely the responsibility of the authors and does not necessarily represent the official views of the National Institutes of Health. The funders had no role in the decision to publish, or preparation of the manuscript.

Appendix A. Supplementary data

Supplementary data to this article can be found online at https://doi.org/10.1016/j.biomaterials.2020.119973.

References

[1] M.F. Pittenger, A.M. Mackay, S.C. Beck, R.K. Jaiswal, R. Douglas, J.D. Mosca, M.A. Moorman, D.W. Simonetti, S. Craig, D.R. Marshak, Multilineage potential of adult human mesenchymal stem cells, Science 284 (1999) 143–147.
[2] D. Noel, D. Caton, S. Roche, C. Bony, S. Lehmann, L. Casteilla, C. Jorgensen, B. Cousin, Cell specific differences between human adipose-derived and mesenchymal-stromal cells despite similar differentiation potentials, Exp. Cell Res. 314 (2008) 1575–1584.
[3] B.P. Hung, J.N. Harvestine, A.M. Saiz, T. Gonzalez-Fernandez, D.E. Sahar, M.L. Weiss, J.K. Leach, Defining hydrogel properties to instruct lineage- and cell-specific mesenchymal differentiation, Biomaterials 189 (2019) 1–10.
[4] Y. Sakaguchi, I. Sekiya, K. Yagishita, T. Muneta, Comparison of human stem cells derived from various mesenchymal tissues: superiority of synovium as a cell source, Arthritis Rheum. 52 (2005) 2521–2529.
[5] A.I. Caplan, J.E. Dennis, Mesenchymal stem cells as trophic mediators, J. Cell. Biochem. 98 (2006) 1076–1084.
[6] S. Meirelles Lda, A.M. Fontes, D.T. Covas, A.I. Caplan, Mechanisms involved in the therapeutic properties of mesenchymal stem cells, Cytokine Growth Factor Rev. 20 (2009) 419–427.
[7] S. Bhumiratana, J.C. Bernhard, D.M. Alfi, K. Yeager, R.E. Eton, J. Bova, F. Shah, J.M. Gimble, M.J. Lopez, S.B. Eisig, G. Vunjak-Novakovic, Tissue-engineered autologous grafts for facial bone reconstruction, Sci. Transl. Med. 8 (2016) 343ra83.
[8] D. Mitra, J. Whitehead, O.W. Yasui, J.K. Leach, Bioreactor culture duration of engineered constructs influences bone formation by mesenchymal stem cells, Biomaterials 146 (2017) 29–39.
[9] J.N. Harvestine, T. Gonzalez-Fernandez, A. Sebastian, N.R. Hum, D.C. Genetos, G.G. Loots, J.K. Leach, Osteogenic preconditioning in perfusion bioreactors improves vascularization and bone formation by human bone marrow aspirates, Sci Adv 6 (7) (2020) eaay2387.
[10] D.L. Hutton, E.M. Moore, J.M. Gimble, W.L. Grayson, Platelet-derived growth factor and spatiotemporal cues induce development of vascularized bone tissue by adipose-derived stem cells, Tissue Eng. 19 (2013) 2076–2086.
[11] A.I. Hoch, B.Y. Binder, D.C. Genetos, J.K. Leach, Differentiation-dependent secretion of proangiogenic factors by mesenchymal stem cells, PloS One 7 (4) (2012) e35579.
[12] A.I. Hoch, V. Mittal, D. Mitra, N. Vollmer, C.A. Zikry, J.K. Leach, Cell-secreted matrices perpetuate the bone-forming phenotype of differentiated mesenchymal stem cells, Biomaterials 74 (2016) 178–187.
[13] A. Bhat, A.I. Hoch, M.L. Decaris, J.K. Leach, Alginate hydrogels containing cell-interactive beads for bone formation, Faseb. J. 27 (12) (2013) 4844–4852.
[14] M.L. Decaris, B.Y. Binder, M.A. Soicher, A. Bhat, J.K. Leach, Cell-derived matrix coatings for polymeric scaffolds, Tissue Eng. 18 (19–20) (2012) 2148–2157.
[15] M.L. Decaris, A. Mojadedi, A. Bhat, J.K. Leach, Transferable cell-secreted extracellular matrices enhance osteogenic differentiation, Acta Biomater. 8 (2) (2012) 744–752.
[16] J.N. Harvestine, N.L. Vollmer, S.S. Ho, C.A. Zikry, M.A. Lee, J.K. Leach, Extracellular matrix-coated composite scaffolds promote mesenchymal stem cell persistence and osteogenesis, Biomacromolecules 17 (11) (2016) 3524–3531.
[17] S.S. Ho, A.T. Keown, B. Addison, J.K. Leach, Cell migration and bone formation from mesenchymal stem cell spheroids in alginate hydrogels are regulated by adhesive ligand density, Biomacromolecules 18 (12) (2017) 4331–4340.
[18] S. Jose, M.L. Hughbanks, B.Y.K. Binder, G.C. Ingavle, J.K. Leach, Enhanced trophic factor secretion by mesenchymal stem/stromal cells with Glycine-Histidine-Lysine (GHK)-modified alginate hydrogels, Acta Biomater. 10 (5) (2014) 1955–1964.
[19] K.Y. Lee, D.J. Mooney, Alginate: properties and biomedical applications, Prog. Polym. Sci. 37 (2012) 106–126.
[20] N. Huebsch, P.R. Arany, A.S. Mao, D. Shvartsman, O.A. Ali, S.A. Bencherif, J. Rivera-Feliciano, D.J. Mooney, Harnessing traction-mediated manipulation of the cell/matrix interface to control stem-cell fate, Nat. Mater. 9 (2010) 518–526.
[21] A. Bauer, L. Gu, B. Kwee, W.A. Li, M. Dellacherie, A.D. Celiz, D.J. Mooney, Hydrogel substrate stress-relaxation regulates the spreading and proliferation of mouse myoblasts, Acta Biomater. 62 (2017) 82–90.
[22] O. Chaudhuri, L. Gu, D. Klumpers, M. Darnell, S.A. Bencherif, J.C. Weaver,

N. Huebsch, H.P. Lee, E. Lippens, G.N. Duda, D.J. Mooney, Hydrogels with tunable stress relaxation regulate stem cell fate and activity, Nat. Mater. 15 (2016) 326–334.
[23] A.H. Van Hove, G.B. Mj, D.S. Benoit, Development and in vitro assessment of enzymatically-responsive poly(ethylene glycol) hydrogels for the delivery of therapeutic peptides, Biomaterials 35 (2014) 9719–9730.
[24] S.S. Mihardja, D. Gao, R.E. Sievers, Q. Fang, J. Feng, J. Wang, H.F. Vanbrocklin, J.W. Larrick, M. Huang, M. Dae, R.J. Lee, Targeted in vivo extracellular matrix formation promotes neovascularization in a rodent model of myocardial infarction, PloS One 5 (2010) e10384.
[25] A. Niemistö, V. Dunmire, O. Yli-Harja, W. Zhang, I. Shmulevich, Robust quantification of in vitro angiogenesis through image analysis, IEEE Trans. Med. Imag. 24 (2005) 549–553.
[26] G. Santulli, M. Ciccarelli, G. Palumbo, A. Campanile, G. Galasso, B. Ziaco, G.G. Altobelli, V. Cimini, F. Piscione, L.D. D'Andrea, C. Pedone, B. Trimarco, G. Iaccarino, In vivo properties of the proangiogenic peptide QK, J. Transl. Med. 7 (2009) 41.
[27] S.S. Ho, K.C. Murphy, B.Y.K. Binder, C.B. Vissers, J.K. Leach, Increased survival and function of mesenchymal stem cell spheroids entrapped in instructive alginate hydrogels, Stem Cells Transl Med 5 (6) (2016) 773–781.
[28] J.L. Madrigal, R.S. Stilhano, C. Siltanen, K. Tanaka, S.N. Rezvani, R.P. Morgan, A. Revzin, S.W. Han, E.A. Silva, Microfluidic generation of alginate microgels for the controlled delivery of lentivectors, J. Mater. Chem. B 4 (2016) 6989–6999.
[29] F. Langenbach, J. Handschel, Effects of dexamethasone, ascorbic acid and beta-glycerophosphate on the osteogenic differentiation of stem cells in vitro, Stem Cell Res. Ther. 4 (2013) 117.
[30] B. Delorme, J. Ringe, N. Gallay, Y.L. Vern, D. Kerboeuf, C. Jorgensen, P. Rosset, L. Sensebé, P. Layrolle, T. Häpupl, P. Charbord, Specific plasma membrane protein phenotype of culture-amplified and native human bone marrow mesenchymal stem cells, Blood 111 (2008) 2631–2635.
[31] S.G. Ball, C.A. Shuttleworth, C.M. Kielty, Vascular endothelial growth factor can signal through platelet-derived growth factor receptors, J. Cell Biol. 177 (2007) 489–500.
[32] W.K. Cheung, D.M. Working, L.D. Galuppo, J.K. Leach, Osteogenic comparison of expanded and uncultured adipose stromal cells, Cytotherapy 12 (4) (2010) 554–562.
[33] K.C. Murphy, M.L. Hughbanks, B.Y.K. Binder, C.B. Vissers, J.K. Leach, Engineered fibrin gels for parallel stimulation of mesenchymal stem cell proangiogenic and osteogenic potential, Ann. Biomed. Eng. 43 (8) (2015) 2010–2021.
[34] J.E. Leslie-Barbick, J.E. Saik, D.J. Gould, M.E. Dickinson, J.L. West, The promotion of microvasculature formation in poly(ethylene glycol) diacrylate hydrogels by an immobilized VEGF-mimetic peptide, Biomaterials 32 (2011) 5782–5789.
[35] F. Finetti, A. Basile, D. Capasso, S. Di Gaetano, R. Di Stasi, M. Pascale, C.M. Turco, M. Ziche, L. Morbidelli, L.D. D'Andrea, Functional and pharmacological characterization of a VEGF mimetic peptide on reparative angiogenesis, Biochem. Pharmacol. 84 (2012) 303–311.
[36] A.I. Caplan, D. Correa, PDGF in bone formation and regeneration: new insights into a novel mechanism involving MSCs, J. Orthop. Res. 29 (2011) 1795–1803.
[37] J.O. Hollinger, C.E. Hart, S.N. Hirsch, S. Lynch, G.E. Friedlaender, Recombinant human platelet-derived growth factor: biology and clinical applications, J Bone Joint Surg Am 90 (Suppl 1) (2008) 48–54.
[38] N. Sato, J.G. Beitz, J. Kato, M. Yamamoto, J.W. Clark, P. Calabresi, A. Raymond, a.R. Frackelton, Platelet-derived growth factor indirectly stimulates angiogenesis in vitro, Am. J. Pathol. 142 (1993) 1119–1130.
[39] J. Karar, A. Maity, PI3K/AKT/mTOR pathway in angiogenesis, Front. Mol. Neurosci. 4 (2011) 51.
[40] S.Y. Cheranov, M. Karpurapu, D. Wang, B. Zhang, R.C. Venema, G.N. Rao, An essential role for SRC-activated STAT-3 in 14, 15-EET-induced VEGF expression and angiogenesis, Blood 111 (2008) 5581–5591.
[41] P. Lindahl, M. Hellstrom, M. Kalen, C. Betsholtz, Endothelial-perivascular cell signaling in vascular development: lessons from knockout mice, Curr. Opin. Lipidol. 9 (1998) 407–411.
[42] W.Y. Su, Y.C. Chen, F.H. Lin, Injectable oxidized hyaluronic acid/adipic acid dihydrazide hydrogel for nucleus pulposus regeneration, Acta Biomater. 6 (8) (2010) 3044–3055.
[43] B.P. Hung, D.L. Hutton, K.L. Kozielski, C.J. Bishop, B.A. Naved, J.J. Green, A.I. Caplan, J.M. Gimble, A.H. Dorafshar, W.L. Grayson, Platelet-derived growth factor BB enhances osteogenesis of adipose-derived but not bone marrow-derived mesenchymal stromal/stem cells, Stem Cell. 33 (2015) 2773–2784.
[44] M. Darnell, S. Young, L. Gu, N. Shah, E. Lippens, J. Weaver, G. Duda, D. Mooney, Substrate stress-relaxation regulates scaffold remodeling and bone formation in vivo, Adv Healthc Mater 6 (2017) 1601185–1601192.
[45] H.J. Kong, D. Kaigler, K. Kim, D.J. Mooney, Controlling rigidity and degradation of alginate hydrogels via molecular weight distribution, Biomacromolecules 5 (2004) 1720–1727.
[46] K.C. Murphy, S.Y. Fang, J.K. Leach, Human mesenchymal stem cell spheroids in fibrin hydrogels exhibit improved cell survival and potential for bone healing, Cell Tissue Res. 357 (1) (2014) 91–99.
[47] S.S. Ho, B.P. Hung, N. Heyrani, M.A. Lee, J.K. Leach, Hypoxic preconditioning of mesenchymal stem cells with subsequent spheroid formation accelerates repair of segmental bone defects, Stem Cell. 36 (9) (2018) 1393–1403.